AMERICAN SOCIETY FOR MICROBIOLOGY | Molecular and Cellular Biology®

RESEARCH ARTICLE

ISLET1-Dependent β-Catenin/Hedgehog Signaling Is Required for Outgrowth of the Lower Jaw

Feixue Li,[a] Guoquan Fu,[a] Ying Liu,[a] Xiaoping Miao,[a] Yan Li,[a] Xueqin Yang,[a] Xiaoyun Zhang,[a] Dongliang Yu,[a] Lin Gan,[a] Mengsheng Qiu,[a] Yiping Chen,[b] Ze Zhang,[c] Zunyi Zhang[a]

Institute of Developmental and Regenerative Biology, College of Life and Environmental Science, Hangzhou Normal University, Zhejiang, China[a]; Department of Molecular Cell Biology, Tulane University, New Orleans, Louisiana, USA[b]; Department of Ophthalmology, Tulane Medical Center, New Orleans, Louisiana, USA[c]

ABSTRACT Mandibular patterning information initially resides in the epithelium during development. However, how transcriptional regulation of epithelium-derived signaling controls morphogenesis of the mandible remains elusive. Using *Shh*^{Cre} to target the mandibular epithelium, we ablated transcription factor *Islet1*, resulting in a distally truncated mandible via unbalanced cell apoptosis and decreased cell proliferation in the distal mesenchyme. Loss of *Islet1* caused a lack of cartilage at the distal tip, leading the fusion of two growing mandibular elements surrounding the rostral process of Meckel's cartilage. Loss of *Islet1* results in dysregulation of mesenchymal genes important for morphogenesis of the mandibular arch. We revealed that *Islet1* is required for the activation of epithelial β-catenin signaling via repression of Wnt antagonists. Reactivation of β-catenin in the epithelium of the *Islet1* mutant rescued mandibular morphogenesis through sonic hedgehog (SHH) signaling to the mesenchyme. Furthermore, overexpression of a transgenic hedgehog ligand in the epithelium also partially restored outgrowth of the mandible. These data reveal functional roles for an ISLET1-dependent network integrating β-catenin/SHH signals in mesenchymal cell survival and outgrowth of the mandible during development.

KEYWORDS *Islet1*, mandibular growth, β-catenin signaling, SHH pathway, epithelium, mesenchyme

Received 6 November 2016 **Returned for modification** 29 November 2016 **Accepted** 4 January 2017

Accepted manuscript posted online 9 January 2017

Citation Li F, Fu G, Liu Y, Miao X, Li Y, Yang X, Zhang X, Yu D, Gan L, Qiu M, Chen Y, Zhang Z, Zhang Z. 2017. ISLET1-dependent β-catenin/hedgehog signaling is required for outgrowth of the lower jaw. Mol Cell Biol 37:e00590-16. https://doi.org/10.1128/MCB.00590-16.

Copyright © 2017 American Society for Microbiology. All Rights Reserved.

Address correspondence to Zunyi Zhang, zunyi_zhang@idrbio.org.

F.L. and G.F. contributed equally to this article.

Development of the mandible (lower jaw) depends on the mutual interactions between the cranio-neural crest (CNC)-derived ectomesenchyme and the overlying epithelium (1, 2). At embryonic day 10 (E10.5) in mouse development, the mandibular arch is prepatterned into a rostral side which participates in dentition formation and a caudal side which gives rise to Meckel's cartilage (3). The mandible first appears as a thin condensation of ectomesenchymal cells in the mandibular prominence at E11.5. These mesenchymal cells proliferate and directly differentiate by intramembranous ossification into the mandibular bone along the proximal/distal axis of the Meckel's cartilage rod by E14.5. Active cell proliferation resides at the rostral symphysis of Meckel's cartilage, contributing to anterior growth of the early developing mandible (3, 4).

The patterning information for the mandible initially resides in the epithelium during early mandibular development (5, 6). Epithelium-derived signals such as bone morphogenetic proteins (BMPs), fibroblast growth factors (FGFs), sonic hedgehog (SHH), and WNT induce autoregulatory positive signaling and mutual inhibitory feedback within and between the epithelium and the mesenchyme to orchestrate the molecular interplay required for lower-jaw outgrowth (5, 7–13). However, the transcrip-

tional basis of initiation of these signals in the epithelium of the early mandible remains unclear (14).

Islet1 (*Isl1*) is an LIM homeodomain-containing transcription factor gene expressed as a marker for patterning and cell type specification in many developmental contexts (15, 16). In the early mandibular arch, *Isl1* is exclusively expressed in the distal epithelium (17, 18). *In vitro* studies have suggested that ISL1 acts in a positive-feedback loop with BMP4 in the distal mandible at and before E10.5 (6, 18, 19). Ectopic gain of *Isl1* in the proximal epithelium, on the other hand, inhibits molar formation with concomitant loss of *Fgf8-Barx1* signaling (18). Deletion of β-catenin in *Isl1*-expressing cells resulted in the loss of epithelial *Fgf8* expression and death of mesenchymal cells (17). ISL1 is thus postulated to regulate development of the mandible through signaling pathways such as β-catenin, FGF, and the BMP regulatory network in mouse development (8, 16, 17, 20). However, the early lethality of homozygous *Isl1* mutants at E9.0 prevented the direct analysis of potential roles for Isl1 in the regulation of mandibular signals. In this study, by deleting *Isl1* in epithelial cells of the distal mandibular arch, we found that the loss mutation of *Isl1* resulted in a uniquely truncated mandible lacking the midline. We showed that the rostral mandible is truncated by increased cell apoptosis and decreased proliferation in the mesenchymal compartment, leading to hypoplastic Meckel's cartilage and rostrally premature intramembranous ossification. Loss of *Isl1* resulted in dysregulation of many mesenchymal signature genes critical for mandibular patterning and outgrowth. Genetic activation of β-catenin and/or hedgehog signal in the mandibular ectoderm of the *Isl1* mutant rescued growth defects. We thus reveal that ISL1 regulation of mandibular morphogenesis is mediated through the β-catenin/SHH signaling network from the epithelium to the mesenchyme.

RESULTS

***Isl1* is required for shaping the lower jaw.** To investigate the role of *Isl1* in mandibular development, we sought to ablate *Isl1* in the mandibular arch at an early stage. Using an $Isl1^{LacZ/+}$ knock-in allele, we demonstrated that the expression of *Isl1* was detectable in distal ectoderm of the mandibular arch as early as E9.5 and E10.5 (Fig. 1A), similar to the findings of previously reported studies (17, 18). In Shh^{Cre}/*R26R* mice, we detected efficient Cre activity in epithelium of the mandibular arch from E9.5 onward (Fig. 1B), suggesting that this Shh^{Cre} line can be used to delete the floxed *Isl1* gene ($Isl1^{fl}$) (21). We crossed Shh^{Cre} to mice carrying the $Isl1^{fl}$ allele. Immunohistochemical analysis using antibodies against ISL1 showed that there is no ISL1 protein production in mice carrying the $Isl1^{fl/fl/ShhCre}$ allele ($Isl1^{Shh\text{-}Cre}$) at and after E9.5, in contrast to the presence of ISL1 in the Shh^{Cre} mice (Fig. 1C, Control).

$Isl1^{Shh\text{-}Cre}$ mice were born at the predicted Mendelian ratio but died at postnatal day 0 (P0). Mutant embryos exhibited severe lower-jaw hypoplasia at E18.5 (100% penetration), in contrast to control mice (Fig. 1D). Skeletal preparations revealed that mandibles in $Isl1^{Shh\text{-}Cre}$ mice were formed proximally but truncated distally (Fig. 1E) such that the two mandibular bones were merged (Fig. 1F). Proximal structures such as molar alveolar bone sacs and three secondary cartilaginous processes, the coronoid, condylar, and angular, were indistinguishable between the $Isl1^{Shh\text{-}Cre}$ mutant and the control (Fig. 1F). Histological analysis of the mutant mandible during odontogenesis showed molar formation with no evidence of incisor initiation throughout mandibular development (Fig. 1G). The earliest defect in the rostral portion was morphologically identifiable at E11.5 in the mutant when it was compared with the control (Fig. 1H). Collectively, these data show that the transcription factor ISL1 is required *in vivo* for the distal outgrowth of the lower jaw.

Ablation of Isl1 in ectoderm leads to the distal truncation of the mandibular bone by disruption of cell survival in the mesenchyme. To gain insight into cellular mechanisms causing distal defects in $Isl1^{Shh\text{-}Cre}$ mandible, we examined cell survival and proliferation on consecutive sections of the early mandibular arch. A terminal deoxynucleotidyltransferase-mediated dUTP-biotin nick end labeling (TUNEL) assay exhibited highly intensified cell apoptosis in the midline mesenchyme in E10.5, but not

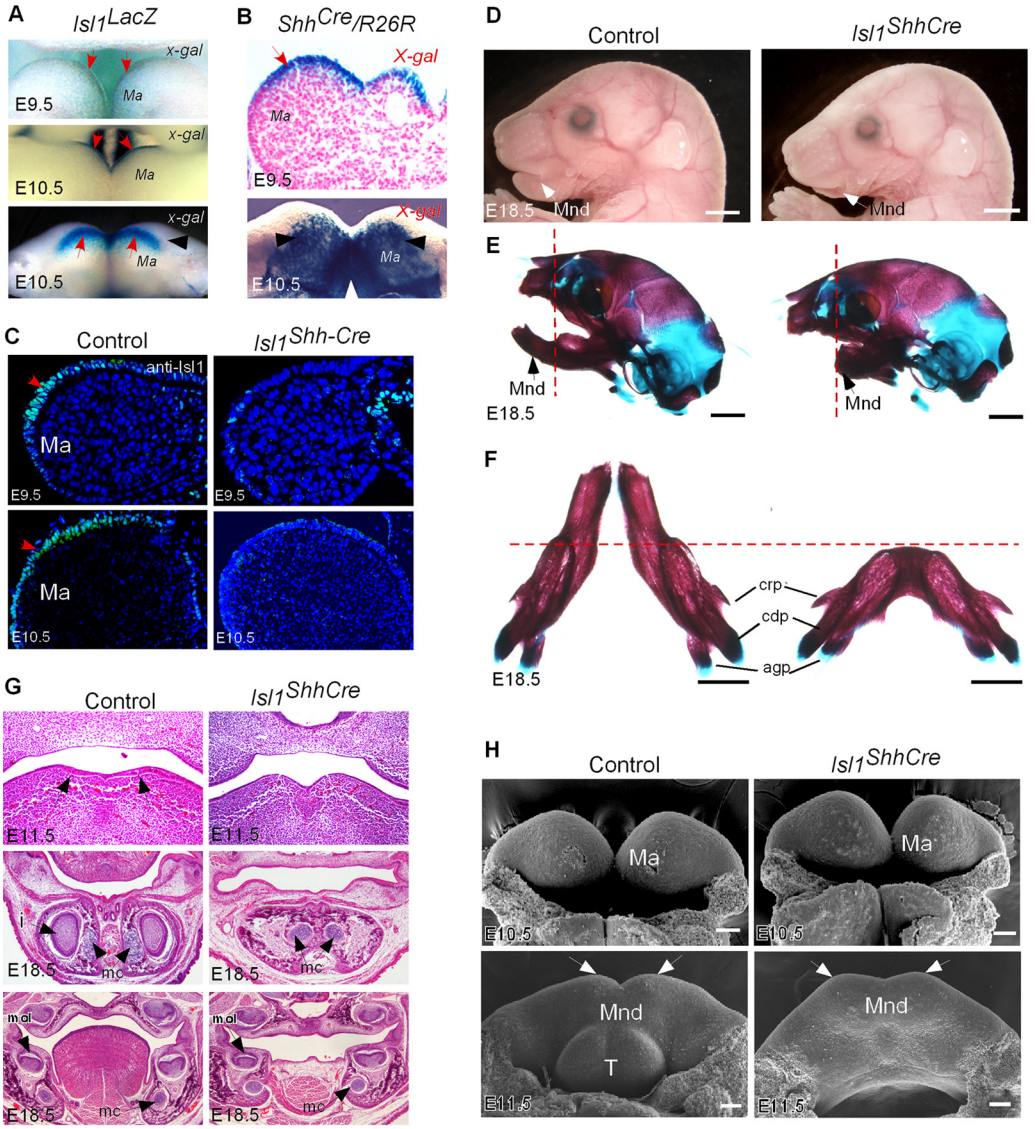

FIG 1 *Isl1* is required for mouse lower jaw patterning and morphogenesis. (A) X-Gal staining showing *Isl1* expression (arrowheads) in $Isl1^{LacZ/+}$ knock-in mice at E9.5 (frontal view) and E10.5 (middle panel for frontal view and bottom panel for oral transverse view). (B) X-Gal staining showing Shh-Cre activity in E9.5 and E10.5 $Shh^{Cre}/R26R$ mandibular arch (arrowheads). (C) Immunofluorescence staining with Islet1 antibody on the sagittal sections of E9.5 and E10.5 mandibles in control (arrowheads) and $Isl1^{Shh\text{-}Cre}$ mice. (D) $Isl1^{Shh\text{-}Cre}$ mouse at E18.5 developed a hypoplastic lower jaw compared to that of the wild type (arrows). (E and F) Skeletal preparations of E18.5 heads (E, lateral view) and E18.5 mandible (F, oral transverse view) stained with alizarin red and alcian blue show mandibular bone fusion and distal truncation (dashed lines). (G) Hematoxylin and eosin staining on the coronal sections of mouse heads showing distal (incisor) and proximal (molar) odontogenesis in Shh^{Cre} and $Isl1^{Shh\text{-}Cre}$ mice. (H) SEM showing the early development of the mouse mandibular arch in Shh^{Cre} and $Isl1^{Shh\text{-}Cre}$ mice. Ma, mandibular arch; Mnd, mandible; crp, coronoid; cdp, condylar; agp, angular. Scale bars, 500 μm (D), 1 mm (E and F), 100 μm (G and H).

E11.5, $Isl1^{Shh\text{-}Cre}$ mandibular arch (Fig. 2A and B), indicating that cell death during an early stage accounts for the loss of this area over 1 day. Deletion of *Isl1* in epithelial cells did not cause abnormal cell death in the epithelium (Fig. 2A and B). Moreover, phospho-histone H3 (pHH3) antibody staining revealed a decrease in proliferation of mesenchymal but not epithelial cells in the distal mandible at E11.5 (Fig. 2C and D). In addition, we detected significant downregulation of cyclin D in the mesenchyme (Fig. 2E), suggesting that loss mutation of *Isl1* resulted in a compromise of mandibular outgrowth through mesenchymal cell proliferation. Taken together, these data suggest that increased cell apoptosis and reduced cell proliferation in the midline mesenchyme in $Isl1^{Shh\text{-}Cre}$ mice cause failed formation of the distal mandible.

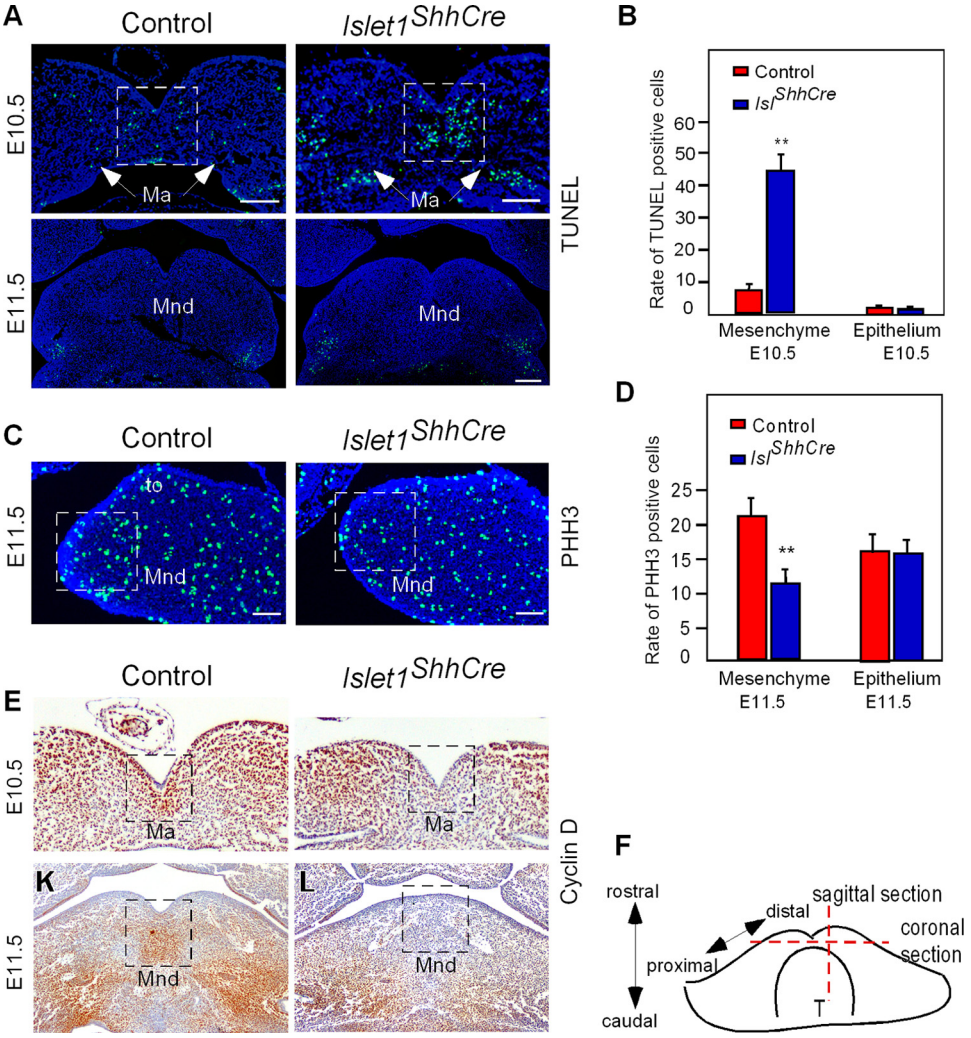

FIG 2 Deletion of *Isl1* in the epithelial cells disrupts cell survival of distal mesenchyme. (A) TUNEL staining on the coronal sections of mandibular prominences at E10.25 and E11.5. (B) Quantification of TUNEL-positive cells in epithelium or mesenchyme versus total epithelial or mesenchymal cells at E10.5 counted from five consecutive fields (presented as boxed areas in panel A). (C) Immunofluorescence with antibody against pHH3 on sagittal sections of the mandible in E11.5 control and Isl1 mutant mice. Boxed areas indicate proliferative cells. (D) Quantification of pHH3-positive cells in epithelium or mesenchyme versus total epithelial or mesenchymal cells (presented as boxed areas in panel C). (E) Immunohistochemical analysis on the sections of the early mandibular arches using antibody against cyclin D. (F) Schematics depicting orientations of histological sections. Dashed lines indicate mandible levels for sagittal and coronal sections. Both rostral/caudal and distal/proximal axes of early E11.0 mandible are indicated by lines with double arrowheads. Plots in panels B and D show the means ± SEM from multiple sections collected from three embryos for each group (**, $P \leq 0.01$). Ma, mandibular arch; Mnd, mandible; Scale bars, 100 μm.

The *Isl1*$^{Shh\text{-}Cre}$ mutant developed a proportionally smaller Meckel's cartilage when it was observed at E13.5 (Fig. 3A). At E14.5 bone and cartilage staining exhibited a well-developed rostral process of Meckel's cartilage that remained undifferentiated in the wild type (Fig. 3A). In the *Isl1*$^{Shh\text{-}Cre}$ mutant, however, bone formation occurred surrounding the rostral process of Meckel's cartilage (Fig. 3A), resulting in an intramembranous bone occupation of the distal mandible, which lacked a midline boundary (Fig. 3A). It may be that loss of the distal mesenchyme caused a lack of cartilage at the distal tip, resulting in fused growth of two ossifying elements. To test whether this is true in the *Isl1*$^{Shh\text{-}Cre}$ mutant, we examined the regulation of Meckel's cartilage primordium by *Sox9* expression (22, 23) and of early osteoblastic cell fate by *Runx2* expression at E11.5. A marked decrease in *Sox9* expression in mandibular mesenchyme was detected by *in situ* hybridization in E11.5 *Isl1*$^{Shh\text{-}Cre}$ embryos (Fig. 3B), attributable to the hypoplastic

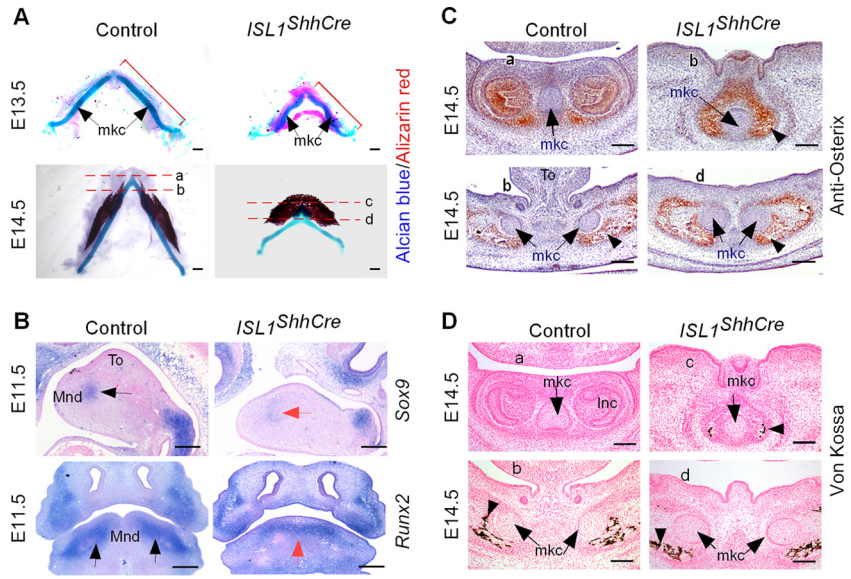

FIG 3 Deletion of *Isl1* leads to an abnormal mandibular phenotype in *Isl1*$^{Shh\text{-}Cre}$ mice. (A) Alcian blue and alizarin red staining for E13 and E14.5 mandibles, shown as dorsal views. The rostral side is toward the upper portion of the image. Dashed lines (a, b, c, and d) represent approximate section levels crossing within and posterior to the rostral process of Meckel's cartilage in panels C and D. (B) *In situ* hybridization in E11.5 mandibular arches using an antisense riboprobe for Sox9 and *Runx2*. (C) Immunohistochemical staining in coronal sections in the E14.5 mandible using antibody against osterix. Note the differentiated osteogenic cells surrounding the rostral process of Meckel's cartilage (arrows) in the *Isl1*$^{Shh\text{-}Cre}$ mutant (arrowheads; $n = 4$). (D) von Kossa staining in E14.5 mandibles shows premature bone mineralization surrounding the rostral process in the *Isl1*$^{Shh\text{-}Cre}$ mutant (arrowheads; $n = 4$). Mnd, mandibular; mkc, Meckel's cartilage; To, tongue. Scale bars: 200 μm (A and B) and 100 μm (C and D).

Meckel's cartilage primordium. In the E11.5 wild-type mandibular arch, transcript of *Runx2* was located around the condensed mesenchyme of Meckel's cartilage primordium (Fig. 3B). In contrast, bilateral expression domains of *Runx2* in the mesenchyme were medially merged in the mutant (Fig. 3B), suggesting ossification in the midline mesenchyme. The spatial relationship between the abnormal bone mineralization and Meckel's cartilage was exemplified by both the osterix expression pattern (Fig. 3C) (24) and von Kossa staining (Fig. 3D). Taken together, these data suggest that the growth deficiencies in the distal mesenchyme resulted in hypoplastic Meckel's cartilage with a lack of the distal tip in the *Isl1*$^{Shh\text{-}Cre}$ mutant, which may cause fused growth of two ossifying bone elements.

Loss of loss of epithelial *Isl1* expression results in differential expression of mesenchymal signature genes critical for mandibular morphogenesis. To verify how the ISL1-dependent distal defect was evoked in the mesenchymal compartment of mutant mandibular arch, we examined the expression pattern of *Barx1* (6), the proximal marker, and *Hand1* and *Hand2*, the mesenchymal markers for distal midline (4). The *Barx1*-expressing region was evidently altered in the E11.5 *Isl1*$^{Shh\text{-}Cre}$ mandible, where the *Barx1* transcript occupied the entire caudal/medial mandible lacking any identifiable expression boundary in the midline (Fig. 4A). This is consistent with the notion that distal mandible was not well established. Moreover, the *Isl1*$^{Shh\text{-}Cre}$ mutant displayed markedly reduced levels of *Hand1* and *Hand2* in midline (Fig. 4A), indicating an impaired development in the mesenchyme. Next, we examined the transcription profile of distal mandibles purified from *Isl1*$^{Shh\text{-}Cre}$ mice and controls at late E10.5 to quantify the genes reflecting a loss of midline mesenchyme in the absence of *Isl1*. We selected this stage because the gene expression pattern change was identifiable in the mutant mandibular arch, but the mesenchymal differentiation of mandibular bone had not yet occurred. RNAs purified from the rostral portions of these two groups were subjected to deep sequencing and bioinformatics analyses. Of 17,806 genes analyzed, 675 protein-coding genes were differentially expressed by $\geq$2.0-fold in the *Isl1*$^{Shh\text{-}Cre}$ mu-

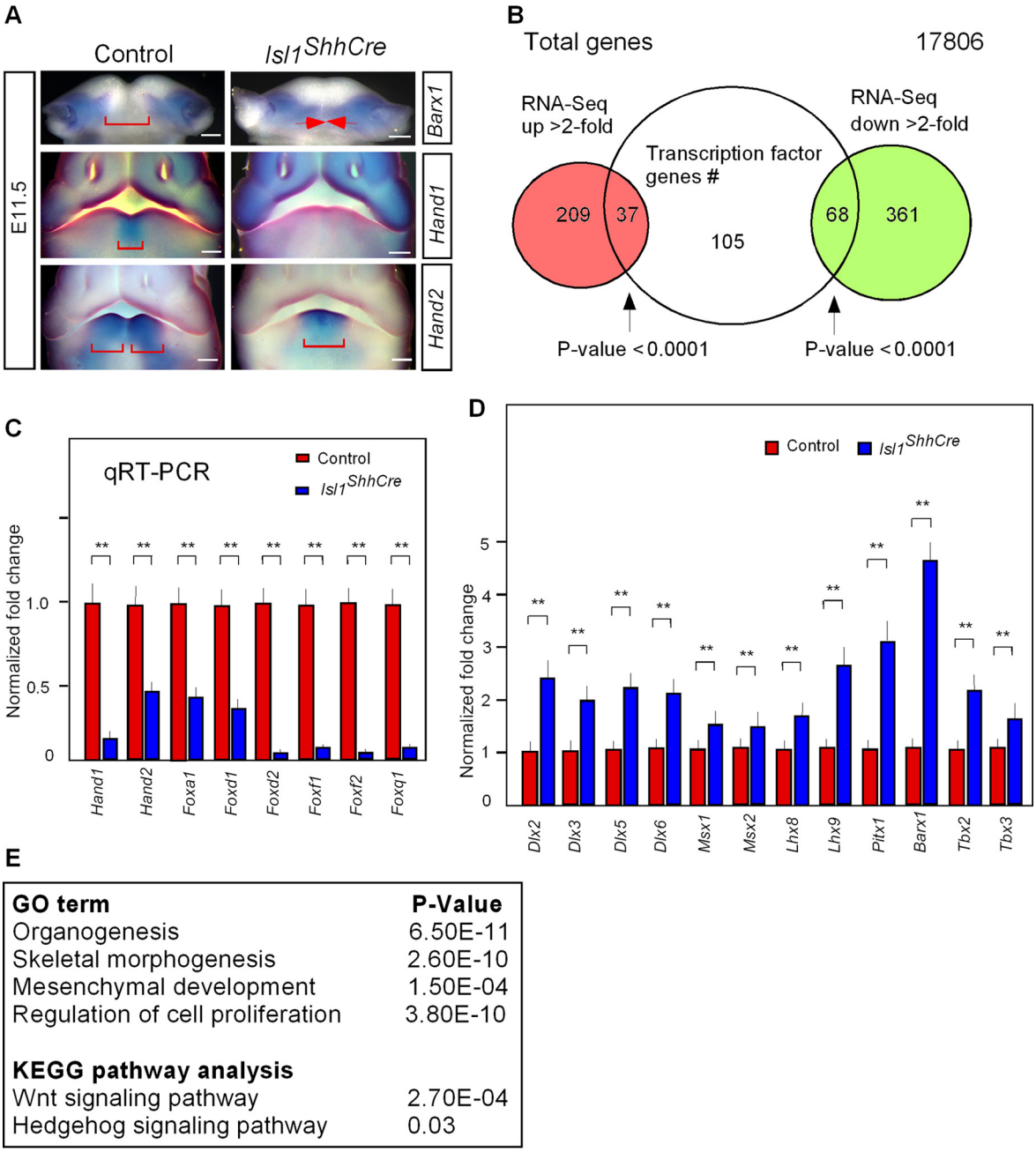

E

GO term	P-Value
Organogenesis	6.50E-11
Skeletal morphogenesis	2.60E-10
Mesenchymal development	1.50E-04
Regulation of cell proliferation	3.80E-10
KEGG pathway analysis	
Wnt signaling pathway	2.70E-04
Hedgehog signaling pathway	0.03

FIG 4 Changes in gene expression in the mandibular mesenchyme of the *Isl1*$^{Shh\text{-}Cre}$ mutant. (A) Whole-mount *in situ* hybridization using riboprobes for and *Barx1* (oral transverse view) and *Hand1* and *Hand2* (frontal views) in *Isl1*$^{Shh\text{-}Cre}$ mandibular arches ($n = 4$), showing changes in transcript domains (bracketed areas). Scale bars, 200 μm. (B) Summary of genes misregulated in E11 *Isl1*$^{Shh\text{-}Cre}$ mandibles. Diagram shows an overlap of transcription factor (TF)-coding genes, differentially expressed, enriched ≥2.0-fold in the *Isl1*$^{Shh\text{-}Cre}$ mutant ($n = 3$) versus the *Shh*^{Cre} control ($n = 3$). Transcription factor-coding genes (#) were retrieved from the Animal Transcription Factor Database (http://www.bioguo.org/AnimalTFDB/index.php). The heat map indicates reduced (green) and increased (red) TF transcripts. (C and D) RNA-seq validation by qRT-PCR of independently derived mandibular arch RNA samples ($n = 3$). Data represent means ± SEM (**, $P \leq 0.01$). (E) Gene ontology (GO) biological annotation and KEGG pathway analyses identified high enrichment scores for the categories indicated.

tant versus the control (Fig. 4B; see also Data Set S1 in the supplemental material). Of 105 differentially expressed transcription factor-coding genes, 68 were downregulated (*P* value of <0.0001), and 37 were upregulated (*P* value of <0.0001) (Fig. 4B and Data Set S1). Among them, mesenchymal signature genes known to be critical for craniofacial development are prominent (Data Set S1); representatives include *Dlx3*, *Dlx5*, *Dlx6*, *Msx1*, *Msx2*, *Foxa1*, *Foxd1*, *Foxd2*, *Foxf1*, *Foxf2*, *Foxp1*, *Hand1*, *Lhx8*, *Lhx9*, *Tbx2*, *Tbx3*, *Sp7*, and *Runx2* (1, 9, 25). Quantitative real-time PCR (qRT-PCR) using RNAs purified from

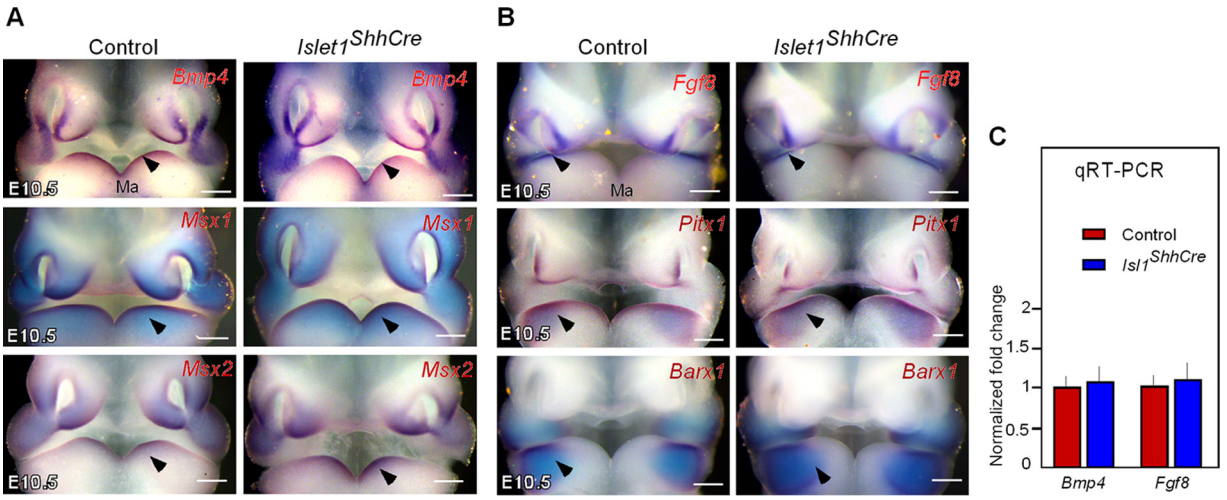

FIG 5 *Bmp4* and *Fgf8* were expressed in *Isl1*$^{Shh\text{-}Cre}$ mandibular arch. (A) Whole-mount *in situ* hybridization showing the expression patterns of *Bmp4*, *Msx1*, and *Msx2 in* E10.5 *Isl1*$^{Shh\text{-}Cre}$ and control (*Shh*^{Cre}) mandibular arches (arrowheads). (B) Whole-mount *in situ* hybridization showing the expression patterns of *Fgf8*, *Pitx2*, and *Barx1* in E10.5 *Isl1*$^{Shh\text{-}Cre}$ and control mandibular arches (arrowheads). (C) Quantitative RT-PCR analysis showing the expression of Bmp4 and Fgf8 in E10.5 *Isl1*$^{Shh\text{-}Cre}$ mandibular epithelium. Error bars represent standard deviations of the PCRs performed in triplicate using two independent samples. Ma, mandibular arch. Scale bars, 100 μm.

independent samples confirmed the altered expression of these mesenchymal genes (Fig. 4C and D). Gene ontology (GO) term analyses revealed that the significantly affected biological processes were enriched in the ISL1-dependent mandibular mesenchyme. In addition to organogenesis, skeletal morphogenesis, and cell regulation, mesenchymal development was among top GO terms (Fig. 4E). Taken together, these data suggest that the expression of all these mesenchymal signature genes is dependent on ISL1 in the epithelium.

A link between ISL1 and secreted signals mediating mesenchymal regulation. Relatively little is known about the mechanism of how an epithelium-localized transcription factor governs the morphogenetic events occurring in the mesenchymal compartment of the mandible. KEGG pathway analyses (Fig. 4E) demonstrated that ISL1-dependent changes in gene expression were associated with secreted signaling molecules.

It was reasonable to suspect that the interruption of an *Isl1-Bmp4* positive loop in the distal epithelium mainly contributes to the aforementioned mandibular truncation in *Isl1*$^{Shh\text{-}Cre}$ mice (1, 6, 18). *In situ* hybridization analysis at E10.5 (n = 8/8), however, did not reveal the sign of disruption in the expression of *Bmp4* in the distal epithelium (Fig. 5A and C) and its targets Msx1 and Msx2 in the distal mesenchyme as well (Fig. 5A), ruling out this possibility in the *Isl1*$^{Shh\text{-}Cre}$ mutant. We also examined the expression of *Fgf8* in proximal epithelium (Fig. 5B and C) and its targets *Barx1* and *Pitx1* in the mesenchyme at E10.5 in the *Isl1*$^{Shh\text{-}Cre}$ mutant (Fig. 5B). Taken together, these data suggest that *Isl1* might not be directly required for onset of *Bmp4* and *Fgf8* expression in E10.5 mandibular ectoderm.

Intriguingly, data from transcriptome sequencing (RNA-seq), confirmed by qRT-PCR analysis on RNA samples extracted from the epithelial compartment of late E10.5 *Isl1*$^{Shh\text{-}Cre}$ mandibular arches, demonstrated an increase in expression of several genes coding the antagonist of Wnt/β-catenin signaling, including *Dkk1*, *Dkk2*, *Dkk3*, and *Wif1* (Fig. 6A and Data Set S1), suggesting the possibility of ISL1 repression of these WNT/β-catenin signaling antagonists (26, 27). In contrast, expression of *Shh* in the mandibular epithelium and its signaling targets, *Ptc1* and *Gli1*, in the mesenchyme was downregulated (Fig. 6A). Together, these findings suggest a link between ISL1 and secreted signaling molecules between the epithelium and the mesenchyme. We thus hypothesized that these secreted signaling molecules might be the downstream targets of ISL1 in the mandibular arch ectoderm through which ISL1 controls the cellular activities of the mesenchyme.

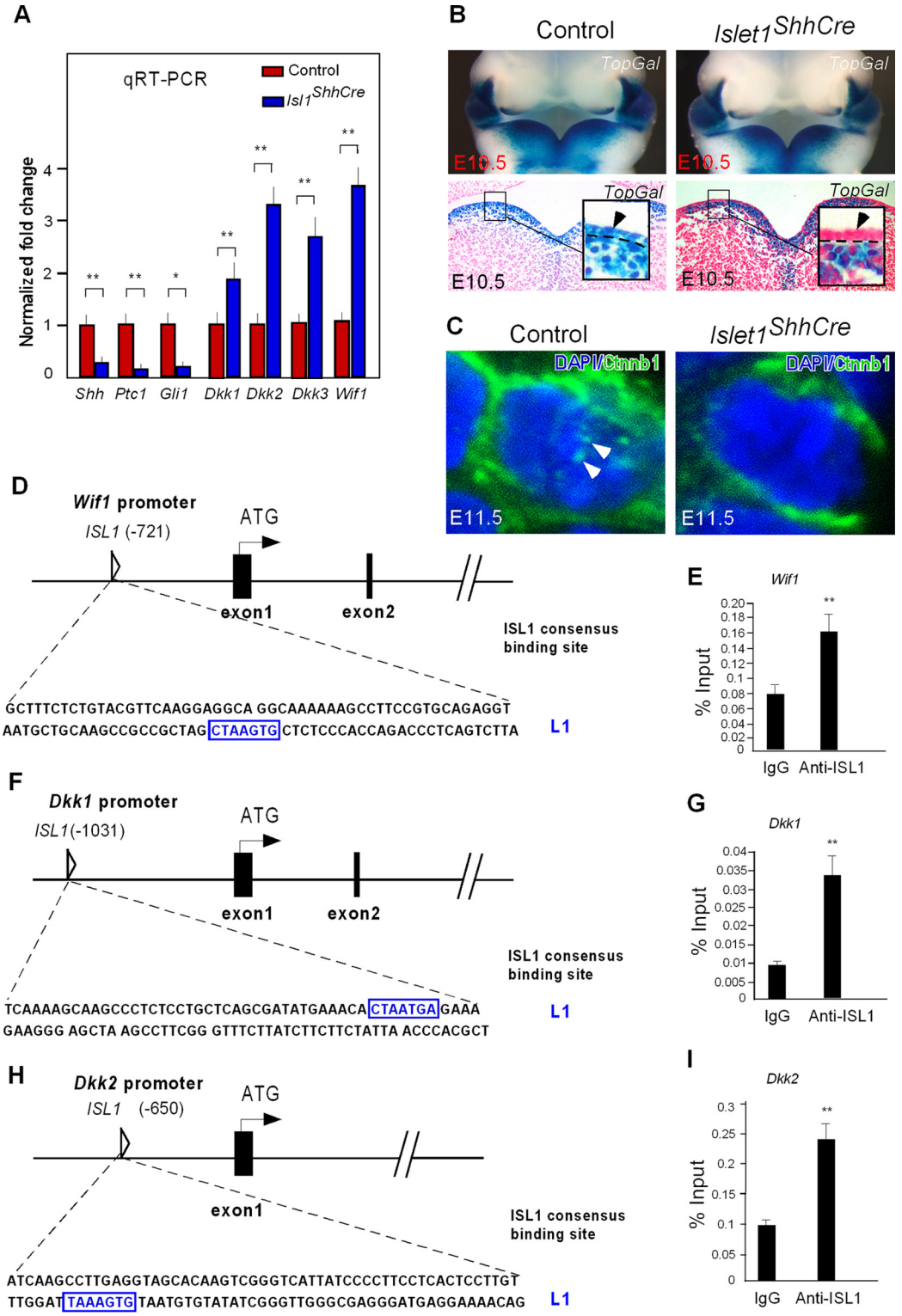

FIG 6 ISL1 sustains the β-catenin pathway via regulation of the Wnt antagonists. (A) Gene expression analyses of SHH pathway and WNT antagonists by quantitative RT-PCR. (B) TOPGAL reporter staining in E10.5 control ($n = 5$) and *Isl1*$^{Shh\text{-}Cre}$ mice ($n = 5$). Note specific inhibition of β-catenin signaling in the ectodermal compartment at E10.5 (arrowheads in insets). Upper panels show frontal views, and lower panels show coronal sections across two mandibular arch prominences. (C) Immunofluorescence of β-catenin in the epithelium of the mandibular arch in E10.5 control ($n = 3$) and *Isl1*$^{Shh\text{-}Cre}$ ($n = 3$) mice. Arrowheads depict the nuclear accumulation. (D to I) Schematic representations of the *Wif1*, *Dkk1*, and *Dkk2* promoter/enhancer regions are shown in panels D, F, and H, respectively. Sequences of the respective ChIP amplicons are shown, and consensus binding sites for ISL1 are highlighted (L1). Quantitative analysis of the ChIP assays was performed by real-time PCR, and results are shown in panels E, G, and I, respectively. Error bars represent standard deviations of the PCRs performed in triplicate using independent samples. Student's *t* test was used for statistical analysis. *, $P \leq 0.05$; **, $P \leq 0.01$.

ISL1 maintains epithelial β-catenin signaling through the repression of Wnt antagonists. Previous studies have demonstrated that ISL1 is critical for the nuclear accumulation of β-catenin during development (17, 20). To assess the role of ISL1 in controlling β-catenin signaling in mandibular morphogenesis, we first examined the impact of *Isl1* ablation on Wnt/β-catenin signaling by detecting TOPGAL (Tcf optimal promoter β-galactosidase) activity as a Wnt/β-catenin signaling reporter in the $Isl1^{Shh\text{-}Cre}$ mandible. Although whole-mount staining hardly showed distinguishable TOPGAL defects in the E10.5 mice (Fig. 6B), detailed examinations of the histological sections uncovered that TOPGAL activity was decreased in the epithelium (Fig. 6B and insets), suggesting a specific effect of *Isl1* loss on β-catenin signaling in the mandibular ectoderm. To verify this effect, we examined nuclear accumulation of β-catenin, a hallmark of this pathway's activation, in the distal epithelium by fluorescent immunostaining. The nuclear β-catenin level in the majority of epithelial cells was diminished in $Isl1^{Shh\text{-}Cre}$ mice (Fig. 6C), consistent with the notion that ISL1 is required for the activation of β-catenin signaling (17, 20). To test the possibility of ISL1 regulation of the WNT/β-catenin pathway via repression of the WNT antagonists, we performed chromatin immunoprecipitation (ChIP) assays using mandibular samples at E10.5. We identified that there are ISL1 consensus binding sites, 5′-(C/T)TAATG(A/G)-3′ and 5′-T AAAGTG-3′ (28, 29), in the regulatory regions of *Dkk1*, *Dkk2*, and *Wif1* (Fig. 6D to I). These results support the hypothesis that ISL1 may repress the expression of these secreted Wnt antagonists by binding to their promoter regions. Together with the reduced nuclear accumulation of β-catenin in the *Isl1* mutant (Fig. 6B and C), these data suggest that ISL1 may partially sustain epithelial WNT/β-catenin signaling through regulation of the expression of WNT antagonists (30).

β-Catenin signaling within the epithelium mediates Isl1 in maintaining outgrowth of the mandible. If it is true that loss of *Isl1* leads to mesenchymal defects via interaction with epithelial β-catenin signaling, then reducing the genetic dosage of β-catenin in $Isl1^{Shh\text{-}Cre}$ mice may worsen the mandibular defect. To test this hypothesis, we introduced a β-catenin loss-of-function mutation to the $Isl1^{Shh\text{-}Cre}$ mutant. Notably, the *Isl1* mutant carrying a heterozygosity for a β-catenin conditional loss allele ($Isl1^{Shh\text{-}Cre}$; $Ctnnb1^{fl/+}$) exhibited more severe mandibular hypoplasia than $Isl1^{Shh\text{-}Cre}$ mice (Fig. 7A), suggesting that ISL1 and β-catenin signaling may functionally interact to control mandibular development. This notion was further supported by our genetic rescue experiment where an active β-catenin allele (with exon 3 flanked by *loxP* sequences) was introduced to the $Isl1^{Shh\text{-}Cre}$ mutant to activate β-catenin signaling in the mandibular ectoderm [$Isl1^{Shh\text{-}Cre}$; $Ctnnb1^{(ex3)fl}$], which well rescued mandibular morphogenesis, with a result comparable to that of the control (Fig. 7A). A TUNEL assay on the sections of early branchial arch demonstrated that the intensified midline cell death in the absence of *Isl1* was recovered when β-catenin signaling was activated in E10.5 $Isl1^{Shh\text{-}Cre}$; $Ctnnb1^{(ex3)fl}$ mice (Fig. 7B). Interestingly, the expression patterns of *Barx1*, *Hand1*, and *Hand2* were well rescued in $Isl1^{Shh\text{-}Cre}$; $Ctnnb1^{(ex3)fl}$ mandibles (Fig. 7C). Collectively, these findings suggest that β-catenin signaling primarily mediates ISL1 in the epithelial compartment critical for mesenchymal development during mandibular outgrowth.

SHH acts downstream of β-catenin signaling in ISL1-dependent mandibular outgrowth. Next, we explored the mechanism by which ISL1 control of β-catenin signaling in epithelium is conducted to the mesenchyme. Analyses by *in situ* hybridization and qRT-PCR, consistent with RNA-seq data, suggest that *Shh* is an ISL1-dependent gene in the epithelium (Fig. 6A and Data Set S1). We found that decreased *Shh* in the ectoderm and its targets *Ptc1* and *Gli1* in the mesenchyme of the $Isl1^{Shh\text{-}Cre}$ mutant were recovered in the $Isl1^{Shh\text{-}Cre}$; $Ctnnb1^{(ex3)fl}$ mandible (Fig. 7D and E). Thus, it is likely that *Shh* in the distal ectoderm could act downstream of the ISL1/β-catenin pathway, signaling to the mesenchyme (7). To test this possibility, we conditionally overexpressed a transgenic (Tg) *Ihh*, a hedgehog ligand activating the same pathway as SHH (31), in the $Isl1^{Shh\text{-}Cre}$ mandibular epithelium (Fig. 8A). *Ihh* expression from this transgenic allele (Tg-*pmes-Ihh*) was tightly controlled by a transcription stop cassette flanked by two *loxP* sites, permitting Cre-mediated activation (32). Skeletal preparations

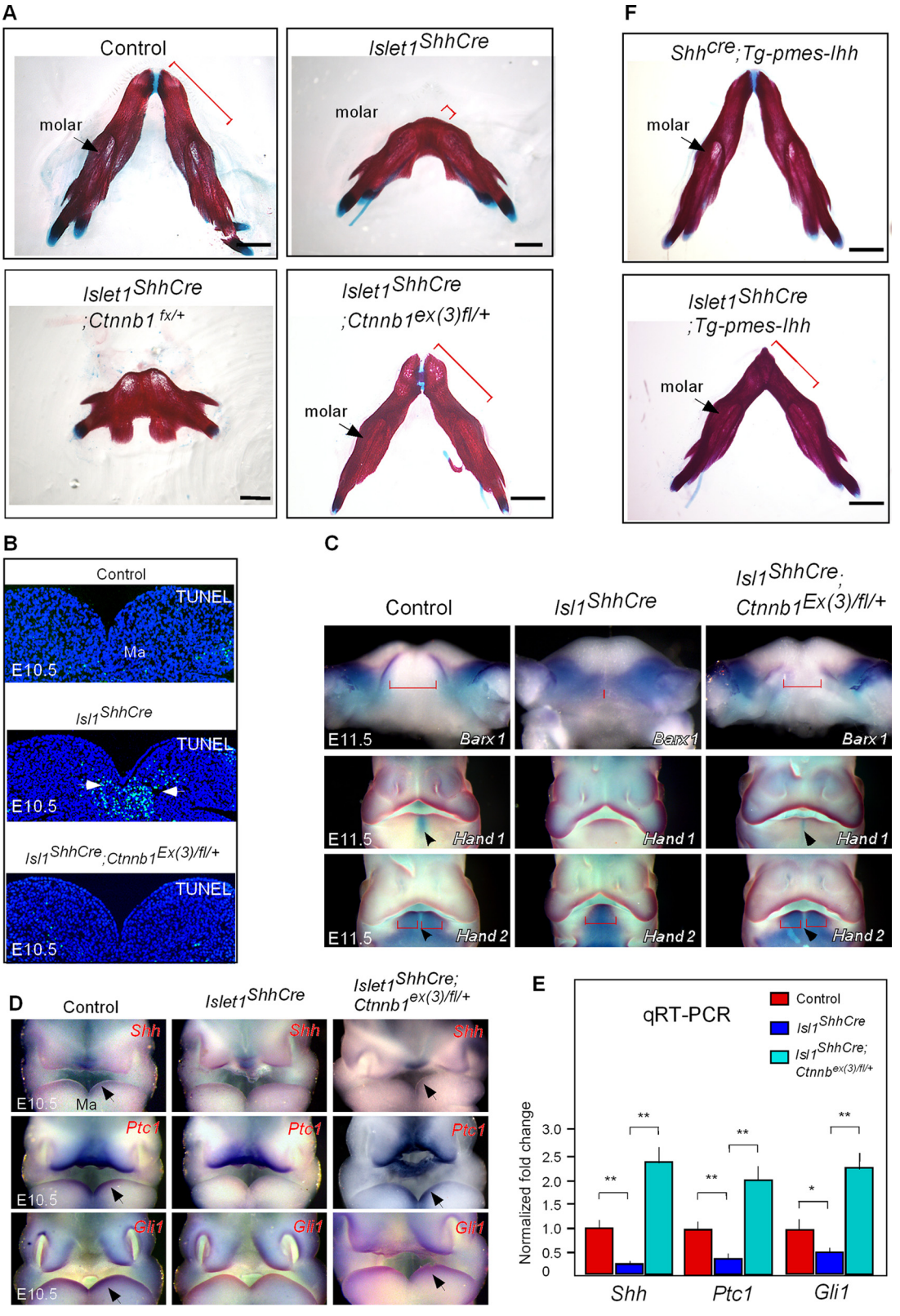

FIG 7 Reactivation of β-catenin signaling rescues mandibular morphogenesis in *Isl1* mutant. (A) Skeletal preparations of control, *Isl1*$^{Shh\text{-}Cre}$, *Isl1*$^{Shh\text{-}Cre}$; *Ctnnb1*$^{fl/+}$, and *Isl1*$^{Shh\text{-}Cre}$; *Ctnnb1*$^{(ex3)fl/+}$ E18.5 mice stained with alizarin red and alcian blue show that in *Isl1*$^{Shh\text{-}Cre}$; *Ctnnb1*$^{(ex3)fl/+}$ mice there is correction of the mandibular truncation seen in the *Isl1*$^{Shh\text{-}Cre}$ mutant. Scale bars, 1 mm. fx, floxed (fl). (B) TUNEL staining on the coronal sections of mandibular arches at E10.5 ($n = 3$). (C) Whole-mount *in situ* hybridization showing the expression pattern restoration of *Barx1* ($n = 5$), *Hand1* ($n = 3$), and *Hand2* ($n = 4$) in the *Isl1*$^{Shh\text{-}Cre}$; *Ctnnb1*$^{(ex3)fl/+}$ mandibular arch. (D) Whole-mount *in situ* hybridization showing reduction in the expression of *Shh*, *Ptc1*, and *Gli1 in* the wild-type control and

(Continued on next page)

revealed that transgenic *Ihh* did alleviate the truncated defect by recovering mandibular outgrowth, resulting in a v-shaped mandible in mice carrying the *Isl1*$^{Shh\text{-}Cre}$; Tg-*pmes-Ihh* allele in contrast to the form in *Isl1*$^{Shh\text{-}Cre}$ mice (Fig. 7F versus A). Moreover, there was also reactivation of *Ptc1* and *Gli1* expression in the mesenchyme (Fig. 8A), indicating that transgenic *Ihh* as a secreted ligand functioned in the mesenchyme. Thus, although hedgehog signaling alone in the mandibular was insufficient to support mandibular patterning and morphogenesis in the absence of *Isl1* and β-catenin signaling, it was able to promote outgrowth by signaling to the mesenchyme and bypassing the ISL1/β-catenin pathway, lending compelling evidence for the genetic integration of β-catenin signaling and the downstream *Shh*.

To further evaluate the impact of activated β-catenin and Shh signaling underlying ISL1 on the development of Meckel's cartilage, we examined the expression of *Sox9* and *Runx2* in E11.5 *Isl1*$^{Shh\text{-}Cre}$; *Ctnnb1*$^{(ex3)fl}$ and *Isl1*$^{Shh\text{-}Cre}$; Tg-*pmes-Ihh* mandibles. We found that activation of β-catenin signaling and overexpression of transgenic *Ihh* rescued the expression patterns of these genes, resulting in patterns comparable to those of the control (Fig. 8B), and were associated with recovered cyclin D in mesenchymal cells (Fig. 8C). Moreover, SHH-saturated beads induced cell proliferation and expression of *Hand1* in mesenchymal cells in *Isl1*$^{Shh\text{-}Cre}$ mandible explants (Fig. 8D), consistent with hedgehog mitogenic activity in mandible development (9).

Finally, we tested the hierarchical relation between *Isl1*, β-catenin signaling, and *Shh* by an *in vitro* mandibular culture system. Knockdown of *Isl1* resulted in downregulation in both *Axin-2* and *Shh* (Fig. 9A), while overexpression of *Isl1* in the *Isl1*$^{Shh\text{-}Cre}$ mandible significantly upregulated their expression (Fig. 9A), consistent with the genetic data that both β-catenin signaling and Shh in the epithelium are downstream of ISL1. Interestingly, treatment with cyclopamine, a natural inhibitor for SHH signaling, or with SHH protein did not produce a significant change in expression of *Axin2* (Fig. 9A), suggesting that β-catenin signaling is not downstream of *Shh*, whereas IWR treatment, which blocks WNT secretion through inhibiting *Porcupine* (33), reduced expression of both *Axin2* and *Shh* (Fig. 9A). In contrast, LiCl treatment resulted in an increase in their expression (Fig. 9A), suggesting that *Shh* is downstream of the β-catenin signaling. This notion is further supported by our ChIP data showing the binding of T cell factor (TCF)/lymphoid enhancer factor 1 (LEF1)/β-catenin complex (34) to the oral epithelial enhancer of the *Shh* gene (35) (Fig. 9B and C). Thus, these *in vitro* results provide further evidence that ISL1 controls the outgrowth of the lower jaw during development through the β-catenin/SHH signaling axis (Fig. 9D).

DISCUSSION

We uncovered in this study that ISL1, as an epithelium-specific transcription factor in the mandibular arch, is required for outgrowth of the distal mesenchyme critical for morphogenesis of the lower jaw. We provide genetic evidence that the β-catenin/SHH signaling network, through a coordinated signaling interplay between the epithelium and the mesenchyme, mediates ISL1-dependent lower jaw shaping.

Our findings shed light on the unrecognized genetic role of ISL1 in regulation of mesenchymal development during mandibular outgrowth. When *Isl1* is ablated in cells of the distal epithelium before the mandibular arch is prepatterned into a rostral and a caudal side (1, 6, 18), the earliest cellular response is significantly enhanced cell death in the midline mesenchyme, where Meckel's cartilage primordium forms at around E11.5 in the mouse. Increased cell death may account for the loss of the distal region of the midline over the next day, resulting in the lack of distal mandibular development.

FIG 7 Legend (Continued)
the *Isl1*$^{Shh\text{-}Cre}$ mutant. Note that the reactivation of hedgehog signaling-related *Ptc1* and *Gli1* is evident in *Isl1*$^{Shh\text{-}Cre}$; *Ctnnb1*$^{(ex3)fl/+}$ mice. (E) Quantitative RT-PCR analysis showing the restoration of SHH signaling in E10.5 *Isl1*$^{Shh\text{-}Cre}$; *Ctnnb1*$^{(ex3)fl/+}$ mandibles. Error bars represent standard deviations of the PCRs performed in triplicate using two independent samples. Student's *t* test was used for statistical analysis (*, $P \leq 0.05$; **, $P \leq 0.01$). (F) Bone staining of E18.5 *Isl1*$^{Shh\text{-}Cre}$; Tg-*pmes-Ihh* mandibles ($n = 3$). Scale bar, 1 mm. Ma, mandibular arch.

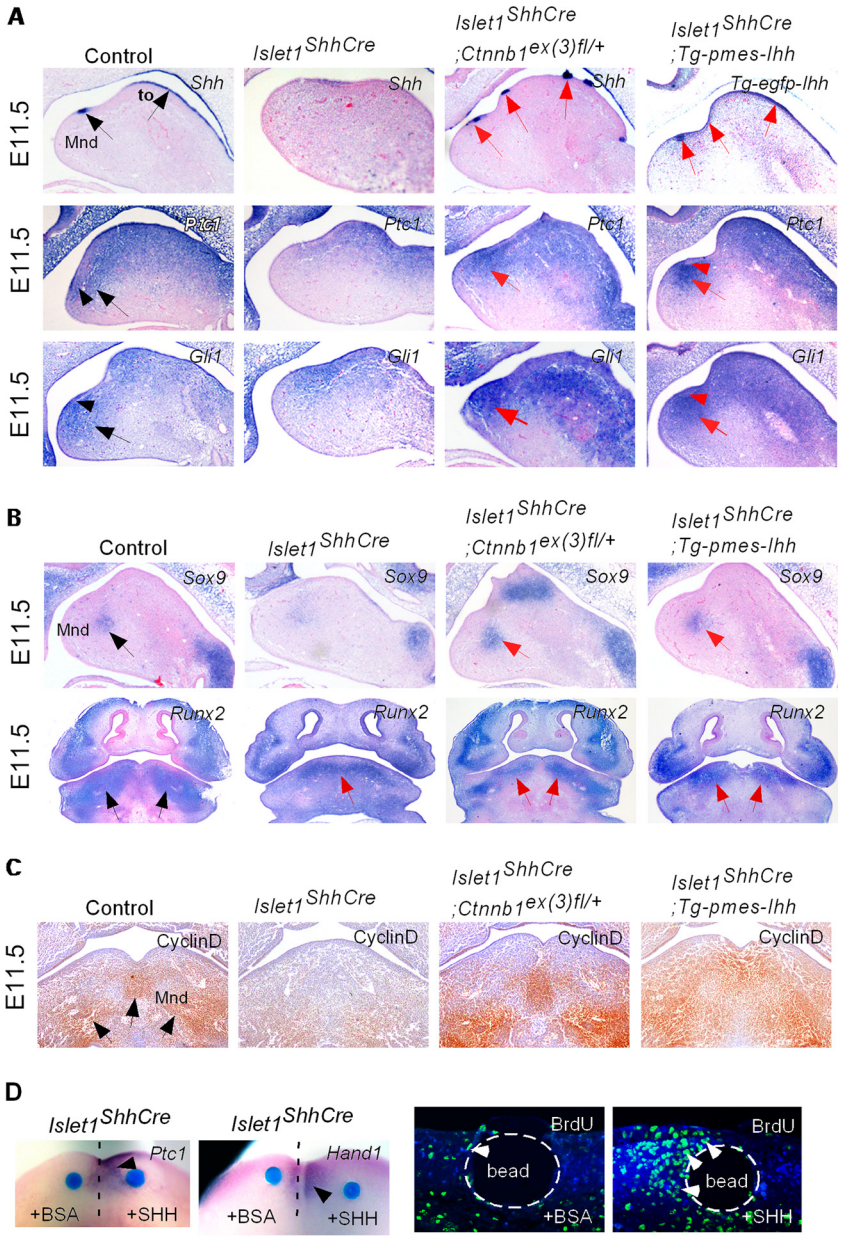

FIG 8 β-Catenin and SHH signaling mediate ISL1 control of mandibular outgrowth. (A) *In situ* hybridization analyses on sagittal sections of mandibular arches. The expression levels of *Shh* in the epithelium and of *Ptc1* and *Gli1* in the mesenchyme (arrows) are rescued in *Isl1*$^{Shh\text{-}Cre}$; *Ctnnb1*$^{(ex3)fl/+}$ and *Isl1*$^{Shh\text{-}Cre}$; Tg-*pmes-Ihh* embryos. Transgenic *Ihh* (arrows) is shown in the mandibular ectoderm (Tg-*Ihh-egfp*). (B) *In situ* hybridization analyses on sagittal (upper row) and coronal (lower row) sections of mandibular arches. The expression levels of *Pax9* and *Runx2* in the mandibular mesenchyme are rescued ($n = 4$) in *Isl1*$^{Shh\text{-}Cre}$; *Ctnnb1*$^{(ex3)fl/+}$ and *Isl1*$^{Shh\text{-}Cre}$; Tg-*pmes-Ihh* embryos. (C) Immunohistochemically data show the restoration of cyclin D expression in *Isl1*$^{Shh\text{-}Cre}$; *Ctnnb1*$^{(ex3)fl/+}$ and *Isl1*$^{Shh\text{-}Cre}$; Tg-*pmes-Ihh* mandibular mesenchyme ($n = 3$). (D) Effect of Shh protein on cell proliferation and Hand1 expression. An SHH-saturated, but not bovine serum albumin (BSA)-saturated, bead induces the expression of *Ptc1* and *Hand1* (arrowheads). Note that SHH protein significantly increased the number of BrdU-positive cells (white arrowheads) compared to the level with the bovine serum albumin control. Mnd, mandible; to, tongue.

In addition, the hypoplastic Meckel's cartilage primordium in the *Isl1*$^{Shh\text{-}Cre}$ mutant could be due to reduced proliferation of cells in mesenchymal condensations, where a reduction of cyclin D level in the mesenchyme was observed by immunohistochemistry. As a result of these cellular defects, Meckel's cartilage appears much shorter because fewer cells are recruited to the mesenchymal condensations, resulting in premature

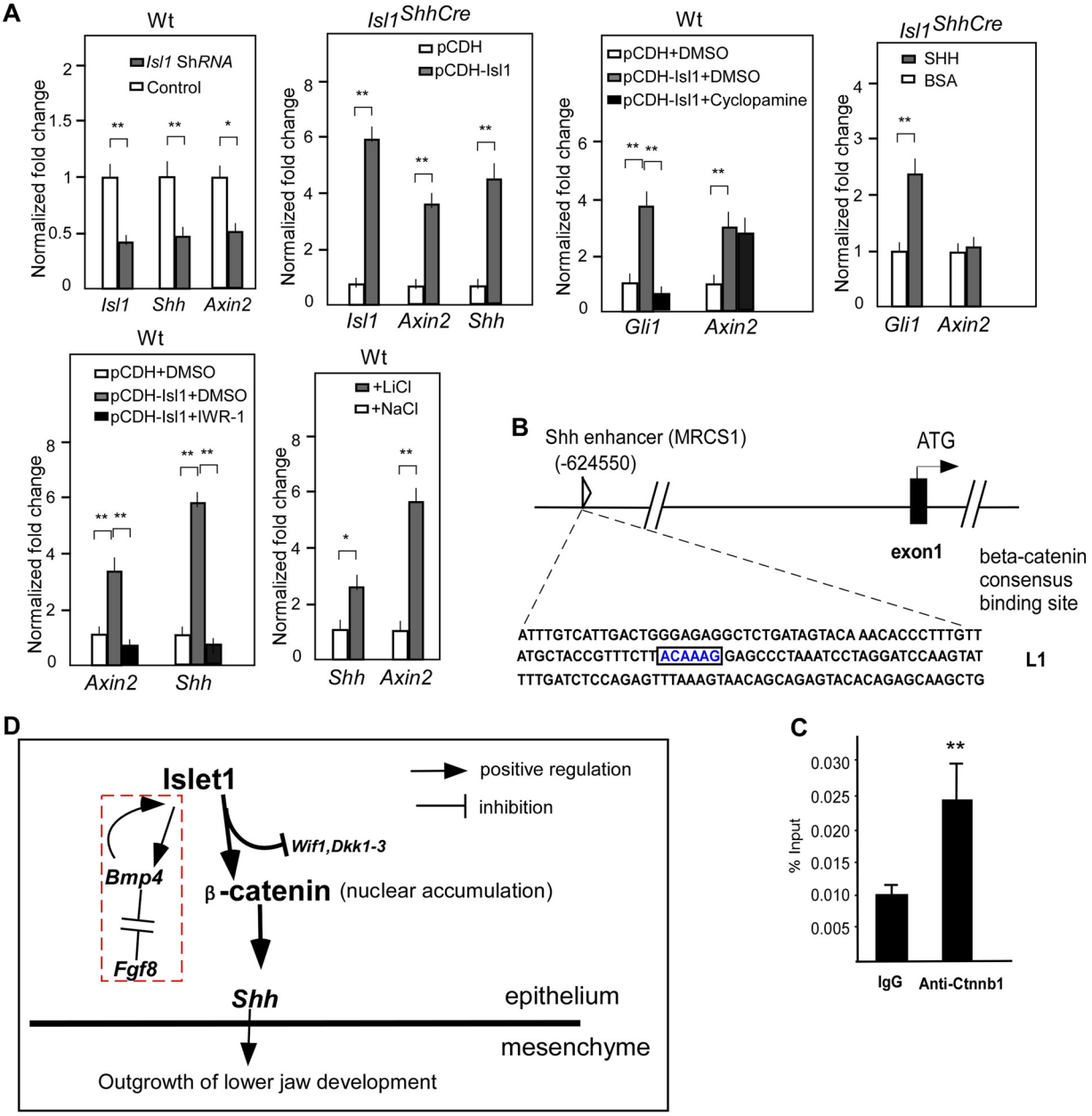

FIG 9 *Shh* is downstream of the β-catenin pathway in the early mandible. (A) Quantitative RT-PCR demonstrates the transcription outcome of the β-catenin pathway and the Shh pathway in mandibular organ cultures. Error bars represent standard deviations of the PCRs performed in triplicate using independent samples. Student's *t* test was used for statistical analysis. *, $P \leq 0.05$; **, $P \leq 0.01$. (B) Schematic representation of the *Shh* oral epithelial enhancer (MRCS1) (35). The sequence of the *Shh* ChIP amplicon is given below, and the consensus binding site for β-catenin is highlighted (L1). (C) Quantitative levels of ChIP assays were analyzed by real-time PCR. Error bars represent standard deviations of the PCRs performed in duplicate using independent samples. Student's *t* test was used for statistical analysis. **, $P \leq 0.01$. (D) Schematic depicts Islet1 regulation of lower jaw morphogenesis through the coordinated interplay of multiple signaling molecules in the ectodermal and the mesenchymal compartments. Note that the pathways in the dashed box have previously been reported (5, 6, 18).

bone mineralization surrounding the tip of the Meckel's cartilage. It is also possible that the marker of cartilage precursor, *Sox9*, responds to *Isl1*-dependent regulation of the distal mesenchyme in the midline of the arch (22, 23). Previous studies have shown that *Sox9*-haploinsufficient neural crest cells failed to properly form Meckel's cartilage primordium, and the precursor of Meckel's cartilage seems to be sensitive to *Sox9* dosage (22, 23, 36). Impaired *Sox9* expression in the rostral mesenchyme accounts for the smaller Meckel's cartilage observed in the $Isl1^{Shh\text{-}Cre}$ mutant, without interference with intramembranous bone formation. Here, we show the role of ISL1 in mandibular

morphogenesis in sustaining distal outgrowth of mesenchyme through regulation of cell survival and proliferation.

Interestingly, the midline defects in the *Isl1*$^{Shh\text{-}Cre}$ mutant partially phenocopy the midline defect in the mutants in which *Hand1* and *Hand2* were ablated. The midline mesenchyme in the mandibular arch, which develops into the interdental mesenchyme and distal symphysis of Meckel's cartilage, is highly sensitive to the dosage of *Hand1* and *Hand2*. Previous studies have demonstrated that, in the mandibular arch, the absence of ventrolateral *Hand2* expression or the reduction of *Hand2*, in combination with the loss of *Hand1*, resulted in a distal mesenchyme defect and eventually led to fusion of the hemi-mandibles and lower incisors (4). Moreover, downregulation of *Hand1* and *Hand2* may compromise their repression of *Dlx5* and *Dlx6* expression and may result in upregulation of *Runx2* and *Sp7* in the distal arch mesenchyme. These data are consistent with previous findings that *Hand2* is required for repression of distal *Dlx* expression in the mandibular mesenchyme critical for the regulation of osteoblast differentiation (25, 37, 38), suggesting that regulation of the ISL1-dependent pathway is critical for proper regulation of midline mandibular development. This proposal is consistent with our RNA-seq data. Thus, our data reveal the importance of epithelial regulation of mesenchymal development in shaping the distal lower jaw.

How might ISL1 in the distal ectoderm alter the regulation of distal mandibular outgrowth? The model we discussed suggests that ISL1 control of mandibular outgrowth is mediated through a β-catenin signaling-dependent network consisting of multiple signals (Fig. 7). Although it was proposed a decade ago that there is an ISL1/BMP4 positive-regulatory loop in the epithelium of the early mouse mandible for dentary prepatterning (6, 8, 18), there is no direct genetic evidence that this signaling loop is involved in lower jaw development (17). Previous study has detected *Isl1* expression in the branchial arch ectoderm prior to the stage when the mandibular arch is prepatterned into the incisor region and molar region (6, 8, 18). When E10.0 wild-type mandibular arches were electroporated with *Isl1* expression vectors, ectopic *Bmp4* expression was seen in the epithelium, indicating that ISL1 may induce *Bmp4*. In contrast, we reveal in this study that *Bmp4* expression is sustained in distal epithelium where Cre-mediated deletion of *Isl1* in the mandibular arch epithelium occurs from E9.5 onward. One explanation for the discrepancy between previous *in vitro* studies and our *in vivo* studies might be that ISL1 regulation of *Bmp4* expression in the distal epithelium is time dependent (5, 6, 10, 19, 39). Although at this time we cannot rule out the possibility of inefficient Cre activity in the early branchial arch ectoderm prior to E9.5, our data of active *Bmp4* expression in the *Isl1*$^{Shh\text{-}Cre}$ mutant support the notion that ISL1 regulation at an earlier phase of *Bmp4* expression in distal mandibular arch epithelium corresponding to the presumptive incisor region is independent of its role in lower jaw morphogenesis.

Previous studies have shown ISL1 activation of β-catenin signaling in the development of muscular structures and branchial arch epithelium (17, 20). Although these studies have provided the immunohistochemical evidence that ISL1 may regulate β-catenin signaling through modulating cellular accumulation of β-catenin, we still do not know how ISL1 as a transcription factor regulates the β-catenin pathway due to lack of mechanical evidence. Given that DKK1 to DKK3 and WIF1 function as antagonists for the activity of WNT/β-catenin signaling (26, 27, 40–42) and that upregulation of WNT antagonists in the absence of *Isl1* results in the reduced accumulation of nuclear β-catenin, we thus suggest that ISL1 is required for the maintenance of the epithelial β-catenin signaling critical for mandibular morphogenesis and growth via repressive regulation of WNT antagonists. Our ChIP assay showing ISL1 binding to the promoter regions of these Wnt antagonists provides partial evidence to support the possibility. This is further supported by our *in vivo* genetic data demonstrating that activation of β-catenin signaling in the mandibular epithelium in the absence of ISL1 rescues the outgrowth of the lower jaw.

Our genetic rescue data show that expression of transgenic *Ihh* in the epithelial compartment results in the partial rescue of mandibular outgrowth, supporting that Hh

signaling in the mandibular mesenchyme acts downstream of the β-catenin pathway for ISL1 regulation of mandibular outgrowth (7, 13, 43). The mandibular mesenchyme in the *Isl1*$^{Shh\text{-}Cre}$ mutant suffered decreased proliferation via the regulation of cyclin D, leading to a severe outgrowth defect. Although a v-shaped Meckel's cartilage forms in the mesenchyme, it is smaller. These results are in line with previous reports on the essential role of SHH signaling in neural crest cells for the outgrowth of the mandible in mice and chicks (9, 44). The ablation of *Smo* in the neural crest mesenchyme led to mandibular hypoplasia and a reduction in the size of Meckel's cartilage (9, 44). However, it is noteworthy that transgenic *Ihh* fails to completely overcome the fusion of the distal skeletal element in the *Isl1*$^{Shh\text{-}Cre}$ mutant. Although IHH and SHH activate through the same signaling pathway, IHH has a specific impact on osteoblast differentiation of mesenchymal cells through upregulation of *Runx2* (45, 46). While transgenic expression of *Ihh* restores hedgehog signaling in the mesenchyme required for mandibular outgrowth, it promotes osteoblast differentiation in the rostral mandible, suggesting that activation of a hedgehog ligand other than *Shh* in the epithelium cannot completely bypass the upstream β-catenin signaling regulation in response to the deletion of *Isl1*. Whether additional signaling pathways downstream of ISL1-dependent β-catenin signaling pathways are simultaneously required to secure the unfused mandibular symphysis in mice remains to be studied in future.

MATERIALS AND METHODS

Mice. All animal experiments were carried out in strict accordance with the Guide for the Care and Use of Laboratory Animals at Hangzhou Normal University and were approved by the Committee on the Ethics of Animal Experiments of (HNLA-2012-018). Mice were maintained on a C57BL/6J background (The Jackson Laboratory). Female mice, 8 to 12 weeks old, were sacrificed by cervical dislocation for embryonic sample collection. All efforts were made to minimize the quantity of mice used.

Constructions of the *Isl1*^{LacZ} mouse line and a conditionally targeted *Isl1* mouse line, *Isl1*^{fl}, have been described previously (21). An *Shh*$^{tm1(EGFP/cre)}$ mouse line was used to induce the tissue-specific deletion of Isl1 in the mandibular ectoderm during embryonic development. Mouse lines of *Shh*$^{tm1(EGFP/cre)}$, *R26R* reporter, TOPGAL transgenic mice, *Ctnnb1*$^{(ex3)fl}$ (47), and *Ctnnb1*^{fl} (*Ctnnb1*^{tm2Kem}/J) were purchased from the Jackson Laboratory, Bar Harbor, ME. The Tg-*pmes-Ihh* mouse line was created by inserting full-length *Ihh* cDNA into a conditional transgenic expression vector as described previously (32, 48). The morning when a vaginal plug was detected was designated embryonic day 0 (E0).

Phenotypic, cellular, and molecular analysis. Mouse embryos were fixed in ice-cold 4% paraformaldehyde (PFA) (pH 7.4), embedded in paraffin, and sectioned at 7 μm for histological and immunohistochemical analyses and *in situ* hybridization. *In situ* hybridization, skeletal staining, 5-bromo-4-chloro-3-indolyl-β-D-galactopyranoside (X-Gal) staining, qRT-PCR, immunohistochemical staining, and scanning electron microscopy (SEM) were performed using standard protocols as described previously (32, 49). Primary antibodies used in this study were commercially purchased: anti-cyclin D1 (ab134175), anti-phospho-histone H3 (3358; Cell Signaling), and antibromodeoxyuridine (anti-BrdU) (B8434; Sigma). Cell apoptosis was evaluated by TUNEL assay using an *In Situ* Cell Death Assay kit according to the manufacturer's instructions (Roche).

***In vitro* organ culture.** Mouse mandibles were carefully dissected from E11.5 wild-type or mutant embryos and placed on a Nuclepore Track-Etch membrane (0.2-μm pore size) in Trowel-type organ culture dishes. LiCl (5 mM), the SHH pathway inhibitor cyclopamine (5 mM), or the Wnt canonical signal pathway inhibitor IWR-1 (10 μM) was applied to the medium. Shh-saturated agarose beads (1 μg/μl) were grafted in the mandible; an *Isl1* overexpression vector (pCDH-Isl1) or *Isl1* short hairpin RNA (shRNA) expression vector (pGreen-*Isl1* shRNA) was transfected with LipoFilter reagent for 6 h. After being cultured for 48 h in a humidified atmosphere of 5% CO_2 at 37°C, the explants were used for RNA extraction and real-time PCR analysis.

ChIP. Chromatin immunoprecipitation (ChIP) analyses from E10.5 mandible tissue samples were performed using a previously described protocol (32). For binding of ISL1 to the *Dkk1*, *Dkk2*, and *Wif1* promoters, ChIP was performed with antibodies against ISL1 (ab20670; Abcam). For binding of β-catenin/TCF complex to the *Shh* oral epithelial enhancer sequence (MRCS1) (35), ChIP was carried out using antibody against β-catenin (ab32572; Abcam) or normal rabbit IgG (A7016; Beyotime).

For detection of the immunoprecipitated *Dkk1*, *Dkk2*, and *Wif1* promoter regions, eluted DNA was used as a template for triplicate quantitative real-time PCR analyses with the following primers specific for ISL1-binding sites (29): *Wif1*, 5′-GCTTTCTCTGTACGTTCAAGG-3′ and 5′-TAAGACTGAGGGTCTGGTGG-3′; *Dkk1*, 5′-TCAAAAGCAAGCCCTCTCC-3′ and 5′-AGCGGTGGGTTAATAGAAG-3′; *Dkk2*, 5′-ATCAAGCCTTG AGGTAGC-3′ and 5′-CTGTTTTCCTCATCCCTCG-3′. For detection of the immunoprecipitated *Shh* oral epithelial enhancer region (MRCS1) (35), the following primers specific for β-catenin-binding sites were used for qRT-PCR: 5′-ATTTGTCATTGACTGGGAGAGG-3′ and 5′-CAGCTTGCTCTGTGTACTCTGC-3′.

RNA-seq analysis and quantitative RT-PCR. RNA-seq was performed using RNA purified from mandibular cells. In brief, mandibular arches were dissected from embryos in the afternoon of embryonic day 10.5. RNA was extracted using TRIzol reagent (Invitrogen, Carlsbad, CA) and quantified using a

NanoDrop 2000 instrument. RNA-seq libraries were established with an Illumina TruSeq RNA sample prep kit and sequenced using an Illumina HiSeq 4000 instrument at a 150-bp read length. Poor-quality reads were trimmed with the following parameters: (i) read length of <25 bp, (ii) more than 50% of the bases with a quality score lower than 10, and (iii) more than 10% of the bases called as N. Expression analysis was performed using RNA-seq by expectation maximization (RSEM), and differentially expressed genes were determined if the false discovery rate (FDR) was ≤0.001 and if the fold change was >2. Clean reads were mapped to the mouse genome (version mm10) using Bowtie (50). GO and KEGG pathway enrichments were performed with in-house developed Perl scripts. *P* values were calculated with a chi-square test. Enrichment was determined to be a *P* value of <0.05.

For gene expression analysis using a quantitative real time-PCR (qRT-PCR) system, total RNA was extracted from the organ culture explants or separated epithelial/mesenchymal compartments from mandibular arches of E10.5 embryos using an RNAqueous-4PCR kit (Ambion). To isolate the epithelial compartment from the mesenchyme, dissected mandibular arches were treated with 0.1% collagenase for 20 min at 37°C; the epithelial compartment was separated from the mesenchyme using forceps under a dissection microscope. cDNA was synthesized from 2 μg of total RNA from each sample using a PrimeScript 1st Strand cDNA synthesis kit (TaKaRa). The synthesized cDNA was diluted to 100 μl, and an aliquot of 2 μl was used as the template in a 20-μl quantitative real-time PCR system. Real-time RT-PCR was performed using the following primer sequences: *Hand1*, 5′-ACATCGCCTACTTGATGGACG-3′ and 5′-CGCCCTTTAATCCTCTTCTCG-3′; *Hand2*, 5′-TCAAGGACCAAAACAACAACC-3′ and 5′-CAGCTTAGCGTGG AGCTACC-3′; *Ptc1*, 5′-AGACTACCCGAATATCCAGCACC-3′ and 5′-CCAGTCACTGTCAAATGCATCC-3′; *Dlx3*, 5′-AGAAAACTCCCCCAAATGAGG-3′ and 5′-ACATGGAAGGAGAAACAGGTCC-3′; *Dlx5*, 5′-AGCCATGTCTGC TTAGACC-3′ and 5′-GACTCTTCTGTCAAACACTCC-3′; *Dlx6*, 5′-TAACCCACACGAGAGTGACC-3′ and 5′-AAT GTCTCCTTCAGAAGCTCC-3′; *Max1*, 5′-CCCTTGCTACACACTTCCTCC-3′ and 5′-AATCTCTTGGCCTCTGCACC-3′; *Msx2*, 5′-TATCAACTCACCCCTGCAAGC-3′ and 5′-ATCCATCCTGGAGTCTGGTCC-3′; *Dkk1*, 5′-GTCAGCTC AATCCCAAGG-3′ and 5′-CAAGGCAATGTAGCACACC-3′; *Dkk2*, 5′-GCCACCTACTCTTCCAAAGC-3′ and 5′-CTCCACATTCTTACCACATCC-3′; *Dkk3*, 5′-CTCCACATTCTTACCACATCC-3′ and 5′-CCCTCGCTGTTGCTAGAA ACG-3′; *Wif1*, 5′-TACCCCACCATCTGAAACG-3′ and 5′-GCCCAGTGATTTATAATGAAGC-3′; *Lhx8*: 5′-TCGAT TACTTCAGACGGTATGG-3′ and 5′-CAAGAAAAGCAGGCAAAGC-3′; *Lhx9*, 5′-CTGGCCGTAGACAAACA GTG-3′ and 5′-CATCTCAGAGGCGGAAATGC-3′; Tbx2, 5′-TCAACTACCAGGGCACCTCC-3′ and 5′-CCAGTTT TCAATGACACTCAAGC-3′; *Tbx3*, 5′-AAACAACGGAAGTCCCATTATCC-3′ and 5′-CACACGAAGCCCTCTACA AGC-3′; *Foxa1*, 5′-ACTCAGTAAAGATGGAAGTGG-3′ and 5′-TGTAAGGTGAAAGCAAAGG-3′; *Isl1*, 5′-ATGAT GGTGGTTTACAGGCTAAC-3′ and 5′-TCGATGCTACTTCACTGCCAG-3′; *Foxd2*, 5′-ATTTATGAAGAGTCTCCAG ACC-3′ and 5′-GATGCTCAAACAGAAAAGC-3′; *Shh*, 5′-AAAGCTGACCCCTTTAGCCTA-3′ and 5′-TGAGTTCC TTAAATCGTTCGGAG-3′; *Foxf2*, 5′-TCAGTAGGACATTTCTTCC-3′ and 5′-CTGTCACAATACTGAGAGC-3′; *Foxd1*, 5′-AAAATCGCCCTATGCTGC-3′ and 5′-CTGGACCTGAGAATCTCTACACC-3′; *Axin2*, 5′-CCACTACATC CACCACCACG-3′ and 5′-CTCTGCTGCCACAAAACTGC-3′; *Foxf1*, 5′-ACTCCAGTGTCTTTCACCTTGC-3′ and 5′-TGAGCCTGAACTACACCAGC-3′; *Barx1*, 5′-CGAAAGCCAAGAAAGGACG-3′ and 5′-TTCATCCTCCGATTTT GATACC-3′; *FoxP1*, 5′-TCTGATGAAGCCAAATATCC-3′ and 5′-CTAAATGAACTCTGCTGACG-3′; *Pitx1*, 5′-GC TACTCCTACAACAACTGG-3′ and 5′-GTCATGGAAGAGATGGAGC-3′; *Gli1*, 5′-CCAAGCCAACTTTATCAGGG-3′ and 5′-AGCCCGCTTCTTTGTTAATTTGA-3′; *Runx2*, 5′-AGGCAAGAGTTTCACCTTGACC-3′ and 5′-GCCCTAAA TCACTGAGGCGAT-3′.

Real-time PCR was performed in triplicate using SsoFast EvaGreen Supermix with a CFX96 real-time PCR detection system (Bio-Rad Laboratories). Data were analyzed with CFX Manager software and are represented as means ± standard errors of the means (SEM). Data from the wild-type sample were set as the control and were normalized to 1.

Statistical analysis. Data were analyzed and statistics were performed (unpaired two-tail Student's *t* test) using Prism, version 5 (GraphPad). Quantitative data are presented as mean values ± standard deviations.

For quantification of cell proliferation, anti-pHH3-positive cells were counted ($n = 3$ to 7 mandible samples, 15 consecutive fields at a magnification of ×40) and calculated as a percentage of antibody-labeled cells and total nuclear-stained cells (4′,6′-diamidino-2-phenylindole [DAPI] positive) otherwise. For quantification of cell apoptosis, TUNEL-positive cells were counted ($n = 3$ to 6 mandible samples, 15 consecutive fields at a magnification of ×40) and calculated as described above.

Accession number(s). RNA-Seq data have been deposited in the NCBI Sequence Read Archive under accession number SRX1452819.

SUPPLEMENTAL MATERIAL

Supplemental material for this article may be found at https://doi.org/10.1128/MCB.00590-16.

DATA SET S1, xls file, 0.4 MB.

ACKNOWLEDGMENTS

We thank all members of Zunyi Zhang lab at the Institute of Developmental and Regenerative Biology, Hangzhou Normal University, for their suggestions during the generation of these data.

This work was supported by grants from the Natural Science Foundation of Zhejiang province (LZ12C12002) and National Natural Science Foundation of China (31371471, 81570941, and 81670971).

REFERENCES

1. Chai Y, Maxson RE, Jr. 2006. Recent advances in craniofacial morphogenesis. Dev Dyn 235:2353–2375. https://doi.org/10.1002/dvdy.20833.
2. Trainor PA. 2005. Specification and patterning of neural crest cells during craniofacial development. Brain Behav Evol 66:266–280. https://doi.org/10.1159/000088130.
3. Ramaesh T, Bard JB. 2003. The growth and morphogenesis of the early mouse mandible: a quantitative analysis. J Anat 203:213–222. https://doi.org/10.1046/j.1469-7580.2003.00210.x.
4. Barbosa AC, Funato N, Chapman S, McKee MD, Richardson JA, Olson EN, Yanagisawa H. 2007. Hand transcription factors cooperatively regulate development of the distal midline mesenchyme. Dev Biol 310:154–168. https://doi.org/10.1016/j.ydbio.2007.07.036.
5. Liu W, Selever J, Murali D, Sun X, Brugger SM, Ma L, Schwartz RJ, Maxson R, Furuta Y, Martin JF. 2005. Threshold-specific requirements for Bmp4 in mandibular development. Dev Biol 283:282–293. https://doi.org/10.1016/j.ydbio.2005.04.019.
6. Tucker A, Sharpe P. 2004. The cutting-edge of mammalian development; how the embryo makes teeth. Nat Rev Genet 5:499–508. https://doi.org/10.1038/nrg1380.
7. Billmyre KK, Klingensmith J. 2015. Sonic hedgehog from pharyngeal arch 1 epithelium is necessary for early mandibular arch cell survival and later cartilage condensation differentiation. Dev Dyn 244:564–576. https://doi.org/10.1002/dvdy.24256.
8. Bonilla-Claudio M, Wang J, Bai Y, Klysik E, Selever J, Martin JF. 2012. Bmp signaling regulates a dose-dependent transcriptional program to control facial skeletal development. Development 139:709–719. https://doi.org/10.1242/dev.073197.
9. Jeong J, Mao J, Tenzen T, Kottmann AH, McMahon AP. 2004. Hedgehog signaling in the neural crest cells regulates the patterning and growth of facial primordia. Genes Dev 18:937–951. https://doi.org/10.1101/gad.1190304.
10. Matsui M, Klingensmith J. 2014. Multiple tissue-specific requirements for the BMP antagonist Noggin in development of the mammalian craniofacial skeleton. Dev Biol 392:168–181. https://doi.org/10.1016/j.ydbio.2014.06.006.
11. Minoux M, Rijli FM. 2010. Molecular mechanisms of cranial neural crest cell migration and patterning in craniofacial development. Development 137:2605–2621. https://doi.org/10.1242/dev.040048.
12. Reid BS, Yang H, Melvin VS, Taketo MM, Williams T. 2011. Ectodermal Wnt/beta-catenin signaling shapes the mouse face. Dev Biol 349:261–269. https://doi.org/10.1016/j.ydbio.2010.11.012.
13. Sun Y, Teng I, Huo R, Rosenfeld MG, Olson LE, Li X. 2012. Asymmetric requirement of surface epithelial beta-catenin during the upper and lower jaw development. Dev Dyn 241:663–674. https://doi.org/10.1002/dvdy.23755.
14. Liu W, Selever J, Lu MF, Martin JF. 2003. Genetic dissection of Pitx2 in craniofacial development uncovers new functions in branchial arch morphogenesis, late aspects of tooth morphogenesis and cell migration. Development 130:6375–6385. https://doi.org/10.1242/dev.00849.
15. Pfaff SL, Mendelsohn M, Stewart CL, Edlund T, Jessell TM. 1996. Requirement for LIM homeobox gene Isl1 in motor neuron generation reveals a motor neuron-dependent step in interneuron differentiation. Cell 84:309–320. https://doi.org/10.1016/S0092-8674(00)80985-X.
16. Yang L, Cai CL, Lin L, Qyang Y, Chung C, Monteiro RM, Mummery CL, Fishman GI, Cogen A, Evans S. 2006. Isl1Cre reveals a common Bmp pathway in heart and limb development. Development 133:1575–1585. https://doi.org/10.1242/dev.02322.
17. Akiyama R, Kawakami H, Taketo MM, Evans SM, Wada N, Petryk A, Kawakami Y. 2014. Distinct populations within Isl1 lineages contribute to appendicular and facial skeletogenesis through the beta-catenin pathway. Dev Biol 387:37–48. https://doi.org/10.1016/j.ydbio.2014.01.001.
18. Mitsiadis TA, Angeli I, James C, Lendahl U, Sharpe PT. 2003. Role of Islet1 in the patterning of murine dentition. Development 130:4451–4460. https://doi.org/10.1242/dev.00631.
19. Tucker AS, Matthews KL, Sharpe PT. 1998. Transformation of tooth type induced by inhibition of BMP signaling. Science 282:1136–1138. https://doi.org/10.1126/science.282.5391.1136.
20. Kawakami Y, Marti M, Kawakami H, Itou J, Quach T, Johnson A, Sahara S, O'Leary DD, Nakagawa Y, Lewandoski M, Pfaff S, Evans SM, Izpisua Belmonte JC. 2011. Islet1-mediated activation of the beta-catenin pathway is necessary for hindlimb initiation in mice. Development 138:4465–4473. https://doi.org/10.1242/dev.065359.
21. Elshatory Y, Everhart D, Deng M, Xie X, Barlow RB, Gan L. 2007. Islet-1 controls the differentiation of retinal bipolar and cholinergic amacrine cells. J Neurosci 27:12707–12720. https://doi.org/10.1523/JNEUROSCI.3951-07.2007.
22. Bi W, Huang W, Whitworth DJ, Deng JM, Zhang Z, Behringer RR, de Crombrugghe B. 2001. Haploinsufficiency of Sox9 results in defective cartilage primordia and premature skeletal mineralization. Proc Natl Acad Sci U S A 98:6698–6703. https://doi.org/10.1073/pnas.111092198.
23. Mori-Akiyama Y, Akiyama H, Rowitch DH, de Crombrugghe B. 2003. Sox9 is required for determination of the chondrogenic cell lineage in the cranial neural crest. Proc Natl Acad Sci U S A 100:9360–9365. https://doi.org/10.1073/pnas.1631288100.
24. Nakashima K, Zhou X, Kunkel G, Zhang Z, Deng JM, Behringer RR, de Crombrugghe B. 2002. The novel zinc finger-containing transcription factor osterix is required for osteoblast differentiation and bone formation. Cell 108:17–29. https://doi.org/10.1016/S0092-8674(01)00622-5.
25. Depew MJ, Simpson CA, Morasso M, Rubenstein JL. 2005. Reassessing the Dlx code: the genetic regulation of branchial arch skeletal pattern and development. J Anat 207:501–561. https://doi.org/10.1111/j.1469-7580.2005.00487.x.
26. Bafico A, Liu G, Yaniv A, Gazit A, Aaronson SA. 2001. Novel mechanism of Wnt signalling inhibition mediated by Dickkopf-1 interaction with LRP6/Arrow. Nat Cell Biol 3:683–686. https://doi.org/10.1038/35083081.
27. Reya T, Clevers H. 2005. Wnt signalling in stem cells and cancer. Nature 434:843–850. https://doi.org/10.1038/nature03319.
28. Karlsson O, Thor S, Norberg T, Ohlsson H, Edlund T. 1990. Insulin gene enhancer binding protein Isl-1 is a member of a novel class of proteins containing both a homeo- and a Cys-His domain. Nature 344:879–882. https://doi.org/10.1038/344879a0.
29. Watanabe Y, Zaffran S, Kuroiwa A, Higuchi H, Ogura T, Harvey RP, Kelly RG, Buckingham M. 2012. Fibroblast growth factor 10 gene regulation in the second heart field by Tbx1, Nkx2-5, and Islet1 reveals a genetic switch for down-regulation in the myocardium. Proc Natl Acad Sci U S A 109:18273–18280. https://doi.org/10.1073/pnas.1215360109.
30. Cao Z, Liu R, Zhang H, Liao H, Zhang Y, Hinton RJ, Feng JQ. 2015. Osterix controls cementoblast differentiation through downregulation of Wnt-signaling via enhancing DKK1 expression. Int J Biol Sci 11:335–344. https://doi.org/10.7150/ijbs.10874.
31. Varjosalo M, Taipale J. 2008. Hedgehog: functions and mechanisms. Genes Dev 22:2454–2472. https://doi.org/10.1101/gad.1693608.
32. Zhu XJ, Liu Y, Dai ZM, Zhang X, Yang X, Li Y, Qiu M, Fu J, Hsu W, Chen Y, Zhang Z. 2014. BMP-FGF signaling axis mediates Wnt-induced epidermal stratification in developing mammalian skin. PLoS Genet 10:e1004687. https://doi.org/10.1371/journal.pgen.1004687.
33. Chen B, Dodge ME, Tang W, Lu J, Ma Z, Fan CW, Wei S, Hao W, Kilgore J, Williams NS, Roth MG, Amatruda JF, Chen C, Lum L. 2009. Small molecule-mediated disruption of Wnt-dependent signaling in tissue regeneration and cancer. Nat Chem Biol 5:100–107. https://doi.org/10.1038/nchembio.137.
34. Wang Y, Song L, Zhou CJ. 2011. The canonical Wnt/beta-catenin signaling pathway regulates Fgf signaling for early facial development. Dev Biol 349:250–260. https://doi.org/10.1016/j.ydbio.2010.11.004.
35. Sagai T, Amano T, Tamura M, Mizushina Y, Sumiyama K, Shiroishi T. 2009. A cluster of three long-range enhancers directs regional Shh expression in the epithelial linings. Development 136:1665–1674. https://doi.org/10.1242/dev.032714.
36. Eames BF, Schneider RA. 2008. The genesis of cartilage size and shape during development and evolution. Development 135:3947–3958. https://doi.org/10.1242/dev.023309.
37. Barron F, Woods C, Kuhn K, Bishop J, Howard MJ, Clouthier DE. 2011. Downregulation of Dlx5 and Dlx6 expression by Hand2 is essential for initiation of tongue morphogenesis. Development 138:2249–2259. https://doi.org/10.1242/dev.056929.
38. Merlo GR, Zerega B, Paleari L, Trombino S, Mantero S, Levi G. 2000. Multiple functions of Dlx genes. Int J Dev Biol 44:619–626.
39. Merrill AE, Eames BF, Weston SJ, Heath T, Schneider RA. 2008. Mesenchyme-dependent BMP signaling directs the timing of mandibular osteogenesis. Development 135:1223–1234. https://doi.org/10.1242/dev.015933.
40. Kawano Y, Kypta R. 2003. Secreted antagonists of the Wnt signalling pathway. J Cell Sci 116:2627–2634. https://doi.org/10.1242/jcs.00623.
41. Malinauskas T, Aricescu AR, Lu W, Siebold C, Jones EY. 2011. Modular mechanism of Wnt signaling inhibition by Wnt inhibitory factor 1. Nat Struct Mol Biol 18:886–893. https://doi.org/10.1038/nsmb.2081.

42. Malinauskas T, Jones EY. 2014. Extracellular modulators of Wnt signalling. Curr Opin Struct Biol 29:77–84. https://doi.org/10.1016/j.sbi.2014.10.003.
43. Sugito H, Shibukawa Y, Kinumatsu T, Yasuda T, Nagayama M, Yamada S, Minugh-Purvis N, Pacifici M, Koyama E. 2011. Ihh signaling regulates mandibular symphysis development and growth. J Dent Res 90:625–631. https://doi.org/10.1177/0022034510397836.
44. Brito JM, Teillet MA, Le Douarin NM. 2006. An early role for sonic hedgehog from foregut endoderm in jaw development: ensuring neural crest cell survival. Proc Natl Acad Sci U S A 103:11607–11612. https://doi.org/10.1073/pnas.0604751103.
45. Lenton K, James AW, Manu A, Brugmann SA, Birker D, Nelson ER, Leucht P, Helms JA, Longaker MT. 2011. Indian hedgehog positively regulates calvarial ossification and modulates bone morphogenetic protein signaling. Genesis 49:784–796. https://doi.org/10.1002/dvg.20768.
46. Shimoyama A, Wada M, Ikeda F, Hata K, Matsubara T, Nifuji A, Noda M, Amano K, Yamaguchi A, Nishimura R, Yoneda T. 2007. Ihh/Gli2 signaling promotes osteoblast differentiation by regulating Runx2 expression and function. Mol Biol Cell 18:2411–2418. https://doi.org/10.1091/mbc.E06-08-0743.
47. Harada N, Tamai Y, Ishikawa T, Sauer B, Takaku K, Oshima M, Taketo MM. 1999. Intestinal polyposis in mice with a dominant stable mutation of the beta-catenin gene. EMBO J 18:5931–5942. https://doi.org/10.1093/emboj/18.21.5931.
48. He F, Xiong W, Wang Y, Matsui M, Yu X, Chai Y, Klingensmith J, Chen Y. 2010. Modulation of BMP signaling by Noggin is required for the maintenance of palatal epithelial integrity during palatogenesis. Dev Biol 347:109–121. https://doi.org/10.1016/j.ydbio.2010.08.014.
49. Zhu X, Zhao P, Liu Y, Zhang X, Fu J, Ivy Yu HM, Qiu M, Chen Y, Hsu W, Zhang Z. 2013. Intra-epithelial requirement of canonical Wnt signaling for tooth morphogenesis. J Biol Chem 288:12080–12089. https://doi.org/10.1074/jbc.M113.462473.
50. Langmead B, Trapnell C, Pop M, Salzberg SL. 2009. Ultrafast and memory-efficient alignment of short DNA sequences to the human genome. Genome Biol 10:R25. https://doi.org/10.1186/gb-2009-10-3-r25.